Front. Struct. Civ. Eng. 2022, 16(8): 1056–1069
https://doi.org/10.1007/s11709-022-0868-3

RESEARCH ARTICLE

Structural optimization of filament wound composite pipes

Roham RAFIEE*, Reza SHAHZADI, Hossein SPERESP

Faculty of New Science and Technologies, University of Tehran, Tehran 1439955171, Iran
**Corresponding author. E-mail: Roham.Rafiee@ut.ac.ir*

ABSTRACT An optimization procedure is developed for obtaining optimal structural design of filament wound composite pipes with minimum cost utilized in pressurized water and waste-water pipelines. First, the short-term and long-term design constraints dictated by international standards are identified. Then, proper computational tools are developed for predicting the structural properties of the composite pipes based on the design architecture of layers. The developed computational tools are validated by relying on experimental analysis. Then, an integrated design-optimization process is developed to minimize the price as the main objective, taking into account design requirements and manufacturing limitations as the constraints and treating lay-up sequence, fiber volume fraction, winding angle, and the number of total layers as design variables. The developed method is implemented in various case studies, and the results are presented and discussed.

KEYWORDS composite pipes, optimization, experimental validation, computational modeling, filament winding

1 Introduction

Glass Fiber Reinforced Polymer (GFRP) pipes play an important role in the infrastructure of countries. Various components of infrastructure, including oil and gas supply,water supply and waste systems, and other utilities, benefit from the unique features of GFRP pipeline systems for conveying potable water, wastewater, oil, gas, or other chemically reactive fluids. Excellent corrosion resistance, high stiffness, outstanding fatigue strength, and favorable hydraulic characteristics have made them a promising alternative to conventional piping systems.

The final price of implementing the GFRP pipeline system is governed not only by the cost of the produced pipes as the short-term indicator but also by the repair and maintenance expenses based on long-term considerations. From the long-term point of view, they are very competitive with other conventional and traditional piping systems mainly because they are not suffering from corrosion. Therefore, the final price of the produced GFRP pipes contributes significantly to the final cost of GFRP pipeline projects. The final price of the GFRP pipes is directly determined by their structural design since configurations of constructive layers define the quantity of raw material consumption.

The structural design pattern of GFRP pipes can fall into two categories: 1) trustworthy pipes with high safety factors but quite unfeasible due to the over-designed scheme; 2) unreliable pipes with economically attractive prices where pre-mature failure is experienced much earlier than design lifetime. Both scenarios are undesirable, and thus industrial producers prefer the first scenario and reduce the cost by decreasing the safety factors through trial-and-error design procedures. Industrial centers practically seek a cost-effective design scenario where all design requirements are fulfilled in parallel with maintaining the price at its minimum possible level. This is strategically a crucial issue to compete in the market with an acceptable profit margin. Consequently, the optimal design is to reach the ideal match among the lifetime, mechanical performance, and cost.

As evidenced by the literature review, aerospace and naval applications were the main areas of optimization studies on cylindrical composites [1]. Thus, the main

Article history: Received Mar 28, 2022; Accepted May 9, 2022

target was to increase either critical buckling loads [2–12] or natural frequencies [13–20] and minimize the weight. Minimal studies have optimized the structural design of GFRP pipes [21–27]. Among them, a few studies have considered different sources of loadings rather than only internal pressure.

Minsch et al. [21] analyzed different aspects of the filament winding process and equipment technology and derived a decision matrix for process engineering to improve the selection of proper equipment for a particular design. A useful analytical tool was provided by Colombo and Vergani [22] for the optimal design of a composite pipe, minimizing the wall thickness by taking into account internal pressure and axial loads. Jin et al. [23] proposed a safety evaluation method based on pipe wall materials' strength and fracture characteristics and suggested a formula to calculate an optimum pipe wall thickness for a pipe undergoing live and dead loads. Almeida et al. [24] proposed a genetic algorithm (GA) to optimize the stacking sequence to improve the strength of a cylindrical shell under internal pressure with and without manufacturing restrictions. Liu and Shi [25] established a model to calculate the winding-induced residual stresses in thick cylinders undergoing internal pressure and optimize the failure pressure. The influences of stacking sequence and fiber orientation on energy absorption in cylindrical composites were studied by Zhang et al. [26], and optimal ply angles were obtained based on finite element modeling and analysis. Two methodologies for optimization of a type III pressure vessel were proposed by Alcántar et al. [27], where weight minimization was the objective function.

The main objective of this article is to develop a systematic and comprehensive approach for optimizing the structural design of GFRP pipes to achieve not only the minimum level of raw material consumption but also proper mechanical performance.

2 Problem statement

It is intended to develop an optimization procedure for obtaining optimal structural design of GFRP pipes with minimum cost for applying pressure water supply. For this purpose, all design requirements dictated by normative standards and manufacturing limitations are considered as the constraints, and the design architecture of composite layers are treated as design variables. Thus, design constraints are first identified. Secondly, proper computational tools for estimating the required structural properties of GFRP pipes are developed and validated. Finally, an optimization process is developed and implemented through developing a computer code. The workflow of the study is shown in Fig. 1, illustrating the involved steps.

3 Computational methods

The structural design of the GFRP pipes in this research aims to be optimized to convey pressurized water/waste water. Hence, design constraints are identified following AWWA C950 [28]. In this section, computational methods used for estimating design constraints are presented. Simple tools are developed for estimating the structural properties of the GFRP pipes. These tools are

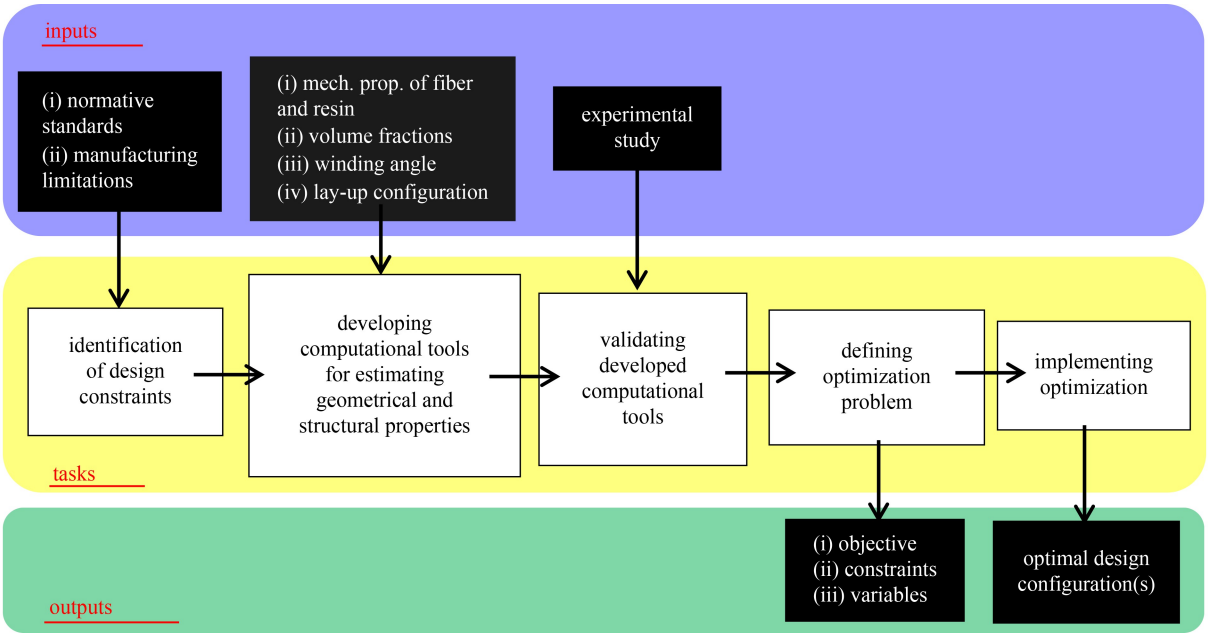

Fig. 1 Workflow of the research.

required to be computationally quick and accurate enough at the same time since the core of the optimization procedure is constructed on them. Before developing necessary computational tools, fundamental parameters must be calculated. Consisting of geometrical specifications and initial mechanical properties of the layers, fundamental tools are input data of the computational tools. Consequently, these fundamental parameters are first explained, and then required computational tools is outlined.

3.1 Fundamental parameters

The structural layers of the GFRP pipes produced through the reciprocal filament winding technique consists of hoop and helical layers. In the hoop layers, the fibers are oriented along circumferential directions. Helical layers are angle plies where the fiber orientation is measured from the axial direction of the pipe. A pair of angle plies in the form of balanced angle plies (i.e., $\pm\theta$) forms a cross-layer. The thickness of each hoop layer is calculated using below formula:

$$t_{\text{hoop}} = \frac{\rho_{\text{A}}^{\text{H}}}{\rho_{\text{FRP}} \times W_{\text{f}}}, \tag{1}$$

where W_{f} , $\rho_{\text{A}}^{\text{H}}$, and ρ_{FRP} are fiber weight fraction, areal density of the hoop layer, and density of composites, respectively. These parameters are calculated as below:

$$\rho_{\text{A}}^{\text{H}} = \frac{N_{\text{S}} T}{B}, \tag{2}$$

$$\rho_{\text{FRP}} = (V_{\text{f}}\rho_{\text{f}} + V_{\text{m}}\rho_{\text{m}}), \tag{3}$$

$$W_{\text{f}} = \frac{V_{\text{f}}\rho_{\text{f}}}{V_{\text{f}}\rho_{\text{f}} + V_{\text{m}}\rho_{\text{m}}}, \tag{4}$$

where N_{S}, T, and B stand for number of fiber strands in the fiber bundle, fiber Tex (i.e., mass of fiber per on km of fiber length) and band width of the fiber bundle, respectively. V_{f}, V_{m}, ρ_{f}, and ρ_{m} denote fiber volume fraction, matrix volume fraction, fiber density, and matrix density, respectively.

The thickness of cross layers is calculated as below:

$$t_{\text{cross}} = \frac{2 \times \rho_{\text{A}}^{\text{C}}}{\rho_{\text{FRP}} \times W_{\text{f}}}, \tag{5}$$

$$\rho_{\text{A}}^{\text{C}} = \frac{N_{\text{S}} T}{B \sin\theta}, \tag{6}$$

where $\rho_{\text{A}}^{\text{C}}$ is areal density of the cross layer and θ is the winding angle in cross layer.

It is widespread to use a core layer made of sand/resin in-between GFRP layers to increase the thickness of the pipe with an economical method. These types of pipes are referred to as GFRP mortar pipes, and they are mostly used as buried pipes. The thickness of this layer is calculated using the below formula:

$$t_{\text{core}} = \frac{\rho_{\text{A}}^{\text{S}}}{\rho_{\text{S}} \times V_{\text{S}}^{\text{core}}}, \tag{7}$$

where

$$\rho_{\text{A}}^{\text{S}} = \frac{m_{\text{S}}}{\pi D L}. \tag{8}$$

In above equations, $\rho_{\text{A}}^{\text{S}}$, ρ_{S}, and $V_{\text{s}}^{\text{core}}$ are areal density of sand/resin layer, density of sand, and sand volume fraction in core layer, respectively. m_{S}, D, and L stand for mass of sand in the full-length of pipe, pipe diameter, and pipe length, respectively.

After calculating the thickness of each layer, it is also required to obtain the mechanical properties of each layer using the following micromechanical rules [29]:

$$E_X = E_{\text{f}} V_{\text{f}} + E_{\text{m}} V_{\text{m}}, \tag{9}$$

$$\vartheta_X = \vartheta_{\text{f}} V_{\text{f}} + \vartheta_{\text{m}} V_{\text{m}}, \tag{10}$$

$$E_Y = E_{\text{m}} \frac{(1 + 2\eta_{\text{T}} V_{\text{f}})}{(1 - \eta_{\text{T}} V_{\text{f}})};\ \eta_{\text{T}} = \frac{\dfrac{E_{\text{f}}}{E_{\text{m}}} - 1}{\dfrac{E_{\text{f}}}{E_{\text{m}}} + 2}, \tag{11}$$

$$G_{XY} = E_{\text{S}} = G_{\text{m}} \frac{(1 + \eta_{\text{T}} V_{\text{f}})}{(1 - \eta_{\text{T}} V_{\text{f}})};\ \eta_{\text{T}} = \frac{\dfrac{G_{\text{f}}}{G_{\text{m}}} - 1}{\dfrac{G_{\text{f}}}{G_{\text{m}}} + 1}, \tag{12}$$

where E, G, and ν are Young's modulus, shear modulus, and Poisson's ratio, respectively. Subscripts of 'f' and 'm' stand for fiber and matrix, respectively.

Treated as an isotropic material and categorized as particulate composites, mechanical properties of the core layer are also calculated using the below formulas [30]:

$$E_{\text{core}} = \frac{(V_{\text{s}}^{\text{core}})^{0.67} E_{\text{m}}}{1 - (V_{\text{s}}^{\text{core}})^{0.33} \left(1 - \dfrac{E_{\text{m}}}{E_{\text{s}}}\right)} + \left(1 - (V_{\text{s}}^{\text{core}})^{0.67}\right) E_{\text{m}}, \tag{13}$$

$$G_{\text{core}} = \frac{(V_{\text{s}}^{\text{core}})^{0.67} G_{m}}{1 - (V_{\text{s}}^{\text{core}})^{0.33} \left(1 - \dfrac{G_{\text{m}}}{G_{\text{s}}}\right)} + \left(1 - (V_{\text{s}}^{\text{core}})^{0.67}\right) G_{\text{m}}, \tag{14}$$

$$\nu_{\text{core}} = \frac{E_{\text{core}}}{2G_{\text{core}}} - 1, \tag{15}$$

where V_s^{core} is sand volume fraction in core layer.

3.2 Estimating *HTS* and *LTS*

HTS and *LTS* stand for the ultimate strength of GFRP pipe in circumferential and axial directions, respectively. The netting method is employed for predicting *HTS* and *LTS* as a quick tool for the composite structures undergoing tensile loading [30]. In netting analysis, only the contribution of fiber is taken into account, and the role of the matrix is ignored. The tensile strength of hoop plies is computed as below:

$$X_{HH} = 2\frac{N_s S_f T}{B}, \tag{16}$$

where S_f is tensile strength of filament, X_{HH} is the tensile strength of hoop plies along hoop direction per unit-width. The reflected coefficient of 2 in Eq. (16) is originated from this fact that each hoop layer in the pipe can be viewed as two Uni-Directional plies around the pipe: one is placed from 12 to 6 o'clock, and another is positioned from 6 to 12 o'clock. The hoop strength of cross plies is also calculated using the below formula:

$$X_{HC} = 2\left(2\frac{N_s S_f T}{B}\right)\sin^2\theta, \tag{17}$$

where X_{HC} is the tensile strength of cross plies along hoop direction per unit-width. Since each cross ply consists of a pair of helical layers, an additional coefficient of 2 in Eq. (17) is considered compared to Eq. (16). Finally, the hoop tensile strength of the pipes is calculated using the below formula considering the contributions of the hoop and helical layers:

$$HTS_{\text{netting}} = V_f\left(\sum_1^p X_{HH} + \sum_1^q X_{HC}\right), \tag{18}$$

where p and q stand for the total number of hoop plies and the total number of cross plies in the pipe structures, respectively.

The strength of helical plies along the axial direction is calculated using the below formula:

$$X_{LC} = 2\left(\frac{N_s S_f T}{B}\right)\cos^2\theta, \tag{19}$$

where X_{LC} is the tensile strength of cross plies along axial direction per unit-width. For calculating the *LTS* of the pipes, only the contribution of cross layers is taken into account. Since netting analysis is employed, the contribution of hoop plies in *LTS* is ignored. Thus, we have:

$$LTS_{\text{netting}} = V_f\left(\sum_1^q X_{LC}\right). \tag{20}$$

3.3 Estimating failure pressure

The maximum allowable internal pressure is known as failure pressure. For thin-walled GFRP pipes (i.e., $t_r/D < 0.1$), the induced hoop stress in a pipe subjected to internal pressure can be estimated using the below formula:

$$\sigma_H \approx \frac{P_N D_i}{2t_r}, \tag{21}$$

where P_N, D_i, and t_r stand for nominal pressure, internal diameter, and thickness of the structural layers without liner, respectively. Substituting σ_H with *HTS* in Eq. (21), the failure pressure can be indirectly estimated based on netting analysis:

$$P_F \approx \frac{2t_r\sigma_H^{failure}}{D_i} = \frac{2HTS_{\text{netting}}}{D_i}, \tag{22}$$

where $\sigma_H^{failure}$ is failure hoop stress.

3.4 Pipe stiffness

Since pipes are subjected to various source of loadings and internal pressure, they should also withstand them. Pipe stiffness is defined as the resistance of the buried pipe against service loads during installation and/or operation. The circular cross-section of pipes is intended to experience ovality under external transverse loadings. The pipe stiffness governs the vertical deflection of the pipe as a structural property. Pipe stiffness plays a key factor in avoiding the negative side effect of pipe cross-section deformation from both hydraulic and structural integrity viewpoints.

The pipe stiffness is generally expressed using the below formula [20]:

$$\frac{E\bar{I}}{D^3} = PS. \tag{23}$$

Considering GFRP pipes as layered structures, a very simple and efficient method in the context of solid mechanics is employed here to estimate the stiffness of GFRP using the reformed shape of Eq. (23) as below [20]:

$$PS = \frac{\sum_{i=1}^{lastply} E_H^i \bar{I}^i}{(D_i + 2NA)^3}, \tag{24}$$

where $\bar{I}$ is centroidal moment of inertia of the cross-sectional area of the wall per unit length. E_H and NA stand for hoop modulus and location of the neutral axis and calculated using the following relations [20]:

$$E_{\mathrm{H}}=\frac{1}{\frac{m^4}{E_{\mathrm{x}}}+\frac{n^4}{E_{\mathrm{y}}}+\frac{m^2n^2}{E_{\mathrm{s}}}-\frac{2\nu_{\mathrm{x}}m^2n^2}{E_{\mathrm{x}}}},\ m=\cos\theta,\ n=\sin\theta, \tag{25}$$

$$A=\frac{\sum_{i=1}^{lastply}E_{\mathrm{H}}^{i}t^{i}\bar{Y}^{i}}{\sum_{i=1}^{lastply}E_{\mathrm{H}}^{i}t^{i}}, \tag{26}$$

$$\bar{Y}^{i}=\frac{t^{i}}{2}+\sum_{m=1}^{i-1}t^{m}, \tag{27}$$

where $\bar{Y}^{i}$ denotes centroid of each layer. It can be realized from Eqs. (24)–(27) that the pipe stiffness also depends on the lay-up sequence of constructing layers.

4 Validation of computational tools

To validate abovementioned computational tools, various GFRP pipes are manufactured using reciprocal filament winding techniques. Then *HTS*, *LTS*, failure pressure, and pipe stiffness are measured using tensile test [31], split-disk experiment [32], hydrostatic test [33], and parallel plate loading [34], respectively. All four testing procedures are shown in Fig. 2.

Mechanical properties of the utilized fiber and resin are inserted in Table 1 based on the technical data sheet of utilized materials in this study. The volume fraction of constituents is also measured through procedure *G* of ASTM D3171 [35], and obtained values are used as input data in corresponding equations (i.e., Eqs. (3), (9)–(14), (18), (20)). The bandwidth of the fiber bundle was adjusted at 180 mm, containing 42 strands.

It is formidable to measure the thickness of cross, hoop, and core plies separately. Thus, the whole thicknesses of all pipes are measured and compared with the summation of all thicknesses, and a perfect agreement was observed for the thickness comparison. Finally, the computational tools are executed, and the results of estimations are compared with experimentally measured values in Tables 2–4.

As shown in Table 2, the results of estimating *LTS* are more accurate than those of *HTS* values, since the measurement of *LTS* is done on a flat specimen rather than ring specimen used for *HTS*. Generally, the error percentage falls below 15% for all cases that are acceptable for this study. In all cases, computational modeling underestimates both *HTS* and *LTS*, and thus the proposed method is categorized as a conservative method.

The results of Table 3 imply the proper accuracy of the solid mechanic method for predicting stiffness. In all cases, estimated stiffness are lower than that of experimental measurement. This can be considered an advantage of the proposed method, avoiding unreliable design schemes through the optimization process.

It is evident from the comparison of the results in Table 4 that the proposed method for calculating failure pressure has good accuracy. But the estimated failure pressure is overestimated. The experimental failure pressure is associated with leakage pressure, while the proposed indirect netting analysis predicts the complete rupture. Because the proposed method is constructed based on estimating *HTS*, and the *HTS* is also associated with the last-ply-failure. Thus, the overestimation in the result is rational. Since the method is very fast in obtaining the results, it can be accepted as a reasonable compromise for optimization. Moreover, for optimization, the input pressure entered by a user as nominal pressure would be automatically enhanced, accounting for long-term behavior considerations, and thus this shortcoming would be overcome. This strategy is explained in the preceding section when long-term behaviors are also considered design constraints.

5 Optimization framework

Three nominal parameters classify GFRP pipes at the design stages as diameter (DN) in millimeter, pressure (PN) in bar and stiffness (SN) in Pascal. Therefore, the objective is to find an optimal structural design for a GFRP pipe with arbitrary {DN-PN-SN} provided by client. The minimum requirements of *HTS* and *LTS* are reflected in normative standards based on the nominal

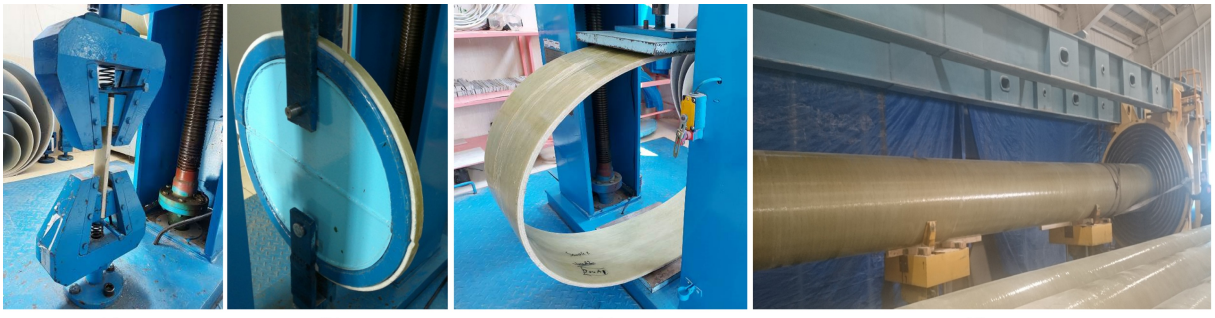

(a) (b) (c) (d)

Fig. 2 Measuring (a) *HTS*; (b) *LTS*; (c) pipe stiffness and (d) failure pressure.

Table 1 Mechanical properties of glass fiber, polyester resin and sand

material	property	value
glass fiber	E_f (GPa)	78
	G_f (GPa)	32
	ν_f	0.22
	S_f (N/Tex)	0.4
	ρ_f (g/m^3)	2.56
polyester resin	E_m (GPa)	3.5
	G_m (GPa)	1.32
	ν_m	0.33
	ρ_m (g/m^3)	1.15
silica sand	E_s (GPa)	10
	G_s (GPa)	3.5
	ρ_s (g/m^3)	2.65

DN and PN of the pipe [28]. The pipe stiffness should also be equal to or greater than nominal SN.

Recalling from Section 3, simple micromechanical rules are used to calculate the pipe layers' mechanical properties. To estimate design constraints, netting analysis is utilized to estimate *HTS*, *LTS*, and failure pressure, and simple solid mechanic theory is utilized for estimating pipe stiffness.

Each GFRP pipe should withstand the hydrostatic test with twice the nominal pressure for a duration of 30 seconds as a quality control test [28]. Therefore, the failure pressure should be more than twice the nominal pressure by default. On the other hand, GFRP pipes for application in water and waste water are required to remain in operation for 50 years as the long-term consideration according to the international rules and regulations [28]. Both remaining pipe stiffness and failure pressure after 50 years should not fall below the nominal

Table 2 Comparing estimated *HTS* and *LTS* with experimental observations

DN (mm)	lay-up	*LTS* (N/mm)		*HTS* (N/mm)	
		netting analysis (error)	experimental	netting analysis (error)	experimental
300	$[90/\pm60.2_2/90]$	139.49 (3.01%)	143.83	1414.43 (5.54%)	1497.44
300	$[90_2/\pm60.2_5/90_3]$	351.5 (2.68%)	361.17	3564.13 (7.31%)	3845.54
500	$[90_2/\pm60.2_4/90]$	204.15 (9.87%)	226.51	1863.48 (13.9%)	2165.2
500	$[90_2/\pm57.5_4/90]$	267.45 (6.38%)	285.69	2012.85 (9.74%)	2230.2
500	$[90_2/\pm60.2_6/90_3]$	391.25 (4.47%)	409.54	3703.25 (8.12%)	4030.55
600	$[90_2/\pm60.2_4/90_2]$	245.33 (8.5%)	268.19	2487.6 (12.4%)	2840.18
500	$[90/\pm60.2/C_{1.17(mm)}/\pm60.2_2/90]$	185.90 (3.28%)	192.22	1634.14 (8.73%)	1790.47

Table 3 Comparing estimated stiffness with experimental observations

DN (mm)	lay-up	stiffness (Pa)	
		solid mechanic method (error)	experimental
300	$[90/\pm60.2_2/90]$	2569 (8.3%)	2800.6
400	$[90/\pm60.2_3/90_3]$	2499 (10%)	2775
500	$[90_2/\pm57.5_4/90]$	4171 (8.2%)	4546.4
600	$[90_2/\pm60.2_4/90_2]$	2091 (7.4%)	2258.3
700	$[90_2/\pm52.5_5/90_3]$	2756 (9.1%)	3031.6
700	$[90/\pm60.2/C_{1.17(mm)}/\pm60.2_2/90]$	2503 (13.4%)	2890.4

Table 4 Comparing failure pressure with experimental observations

DN (mm)	lay-up	failure pressure (MPa)	
		indirect netting analysis (error)	experimental
300	[90/±60.2/90]	6.23 (11.05%)	5.61
300	[90/±60.2]	4.35 (8.2%)	4.02
300	[±60.2]	2.63 (6.91%)	2.46
400	[90/±60.2]	3.38 (10.82%)	3.05
400	$[\pm52.5/C_{1.04(mm)}/90/\pm52.5]$	4.41 (6.5%)	4.72

values. For this reason, a series of long-term experiments are required to be conducted for each type of pipe for a duration of 10000 hours. The obtained results are extrapolated to 50 years, and the remaining pressure/stiffness is estimated [36,37]. In this research, another constraint is proposed to cover both short-term and long-term considerations for the failure pressure. Namely, the nominal pressure entered by the user is enhanced by some correction factors. This strategy can also overcome the shortcoming of indirect netting analysis, where failure pressure was overestimated in Section 5. For long-term stiffness, a similar strategy is considered for the sake of simplicity. All the constraints considered in the optimization process of this research are presented in Table 5, accompanied by objective and design variables. Thus, the optimization problem is outlined in Table 5.

Reflected manufacturing constraints in Table 5 resemble the limitations of the reciprocal filament winding technology utilized in this study, and they are obtained through the practical experience of production. Aforementioned values are subjected to change for other machinery, and thus, these values can be customized. Given the minimum wall thickness as 6 mm originated from the practical experience of manufacturing, GFRP pipes with a thickness of less than 6 mm are highly susceptible to experience buckling either during the hydrostatic test or during extracting the mandrel. Although the occurrence of buckling during mandrel extraction can be avoided using collapsible mandrels, the former persists.

Rafiee and Ghorbanhosseini have done experimental and theoretical studies on long-term stiffness and found that initial stiffness is reduced by about 30% after 50 years [38–40]. Thus, C_{SL} is considered as 1.25 in this research. C_{PL} is also assumed as 1.8 based on the simulation performed for the long-term hydrostatic test [41,42]. It is worth mentioning that C_{SL} and C_{PL} are required to be obtained through experimental tests for each pipe, and suggested values in this research are provided to conduct an optimization process without loss of generality. Explicitly stated in normative standards, long-term experiments as qualification tests should be conducted to approve the structural design of GFRP pipes.

An in-house computer code is written on the Visual Basic platform, where all computational procedures are included. The code requires entering {DN-PN-SN} by the user, and then it starts generating possible structural designs fulfilling the requirements of all constraints. Then direct search method is utilized to find the optimal design(s) based on the defined objective. The direct search method is chosen as a simple tool among various gradient-free optimization methods [43–46]. Therefore, the efficiency of the optimization method is not required to be discussed, since all possible alternatives are generated and evaluated.

Users can adjust all input data, including mechanical properties and the ranges of winding angle, fiber volume fraction in GFRP layers, and sand volume fraction in the core layer. The code has also powered with this feature to design and optimize GFRP pipes or GFRP mortar pipes (containing core layer). The optimization framework is limited to the case of composite pipes for water or wastewater application according to the identified design constraints. As the main assumptions of the modeling, thin-walled structures, and linear behaviors are assumed.

In this research, topology optimization [47,48] is not utilized, since topology optimization results might be challenging to manufacture. Thus, topology optimization is not used in this research, assuring the manufacturability of the optimal design as the output of this research.

6 Results and discussion

In this section, the code is implemented for various case

Table 5 Overview of optimization problem

scope	definition
objective design constraints	minimizing total wall thickness ($t_{hoop} + t_{cross} + t_{core}$)
	(HTS, LTS) ⩾ values in Ref. [28] based on DN and PN
	$P_F \geqslant 2.C_{PL} \cdot PN$
	$PS \geqslant C_{SL} \cdot SN$
manufacturing constraints	$\theta \in [50°, 70°]$
	$W_f = [73\%, 77\%]$
	$V_s = [45\%, 55\%]$
	total wall thickness ⩾ 6 mm
design variables	1) No. of hoop layers (p); 2) No. of cross layers (q); 3) winding angle (θ); 4) mass of sand (m_s); 5) lay-up sequence
input parameters by user	mechanical properties of fiber, resin and sand
	DN-PN-SN
	C_{PL} and C_{SL}

studies, and the results are presented. For each case, the user can define the starting values for the hoop number and cross layers (i.e., p and q) as the starting point based on the design background referred to as the knowledge of expert (KOE). Usually, this information is practically available based on either previous experience of a designer or old design configurations. If such information is not accessible, the user can adjust starting values for the number of hoop and cross layers to 0 and 1, respectively, as the minimum possible number of layers. In other words, the code can find the optimal design even without starting point of search (i.e., KOE), but the runtime significantly decreases employing KOE. To reduce the runtime without KOE, a meta-heuristic optimization technique must be utilized, which is the subject of another research on composite pipes by the first author and his co-workers.

The optimization procedure is first executed for simple cases where some design parameters are unchanged, resembling restricted optimizations. Then, the optimization problem smoothly switches to more complicated cases where no restriction is pertinent to the design variables. This strategy has been taken to trace the outputs of the optimization for verification. Different implemented optimization scenarios are shown in Fig. 3. As is shown, scenarios "A" to "D" belong to GFRP pipes, and scenarios "E" and "F" are related to GFRP mortar pipes. Moreover, all scenarios except scenarios "D" and "F" are carried out based on KOE. Consequently, the restrictions are removed in a step-by-step process through the scenarios "B" and "C" and finally, scenario "D" is implemented without KOE for GFRP pipes.

Scenarios "A" to "D" are implemented on a {600-16-1000} GFRP pipe as a case study. As an additional case study, scenario "D" is also implemented on a {800-6-2500}. Scenarios "E" and "F" are executed for the GFRP mortar pipe with {600-16-4000} specification. The detailed outputs of all scenarios accompanied by initial settings are presented in Table 6. Scenario "A" is implemented based on available KOE, and the obtained results are extensively discussed in the proceeding parts. The required runtimes for the accomplishment of each optimization scenario are also reported in Table 6. All cases were executed on a computer equipped with 16-GB memory and a Core i7-1065G7 processor running at 1.5 GHz frequency.

6.1 Scenarios "A" and "B"

For implementing scenario "A", the total number of layers is chosen as 7 layers, and the weight fraction of fiber is assumed as 73%. Winding angle for cross layers is also selected as 60° based on available KOE. For scenario "A", just 23 outputs among the 128 alternatives of design patterns fulfill the design and manufacturing constraints requirements. The generated design patterns fall into three main categories with three distinct overall thicknesses based on the combinations of the number of hoop and cross layers. As mentioned earlier, the lay-up sequence does not change the *HTS*, *LTS*, and failure pressure. Therefore, generally, three distinct values are presented for the aforementioned categories.

In contrast, pipe stiffness (SN) depends on the lay-up sequence, and thus three different ranges of estimated stiffness are presented in Fig. 4. As expected, increasing the pipe thickness, the pipe's stiffness also increases, and the increasing the number of hoop and/or cross layers, *HTS* also increases. For scenario "A", the optimal designs with the thickness of 6.9 mm belong to the combination of two hoops and five cross layers. Among these combinations, the highest stiffness is achieved by the lay-up sequence of $[90/\pm60_5/90]$ as 1919 Pa.

For scenario "B", the winding angle is also added to the list of design variables and the other design variables assumed in scenario "A". Different values for winding angles are reflected in Table 5. For scenario "B", 261

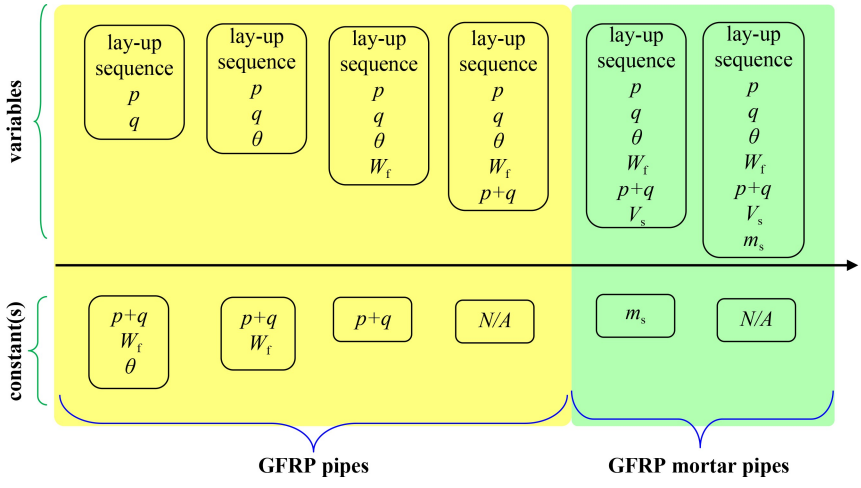

Fig. 3 Description of optimization scenarios for the verification purpose.

Table 6 Outputs of optimization procedure for different scenarios

scenario	constant				outputs							
	m_s (kg)	$p+q$	θ	W_f	lay-up config.	SN (Pa)	*HTS* (N/mm)	*LTS* (N/mm)	P_f (bar)	W_f	m_s (kg)	t (mm)
scenario A[a] runtime = 1.5 min	0	7	60°	73%	$[90/\pm60_5/90]$	1919	2276	299	76	–	–	6.9
					$[\pm60_5/90_2]$	1873						
					$[\pm60/90/\pm60_4/90]$	1769						
					$[\pm60_4/90/\pm60/90]$	1745						
					$[90/\pm60_4/90/\pm60]$	1713						
					$[\pm60_2/90/\pm60_3/90]$	1691						
					$[\pm60_3/90/\pm60_2/90]$	1683						
					$[90_2//\pm60_5]$	1598						
					$[90/\pm60_3/90/\pm60_2]$	1578						
					$[\pm60_4/90_2/\pm60]$	1570						
					$[90/\pm60/90/\pm60_4]$	1521						
					$[90/\pm60_2/90/\pm60_3]$	1514						
					$[\pm60/90_2/\pm60_4]$	1401						
					$[\pm60_3/90_2/\pm60_2]$	1388						
					$[\pm60_2/90_2/\pm60_3]$	1331						
scenario B[a] runtime = 7 min	0	7	–	73%	$[\pm57.5_4/90_3]$	1605	2082	277	69	–	–	6.5
					$[\pm57.5_3/90_3/\pm57.5]$	1251						
					$[90_2/\pm57.5/90/\pm57.5_3]$	1252						
					$[90_3/\pm57.5_4]$	1269						
					$[\pm57.5_2/90_2/\pm57.5_2/90]$	1360						
					$[\pm57.5_3/90_2/\pm57.5/90]$	1414						
					$[\pm57.5/90_2/\pm57.5_3/90]$	1443						
					$[90_2/\pm57.5_3/90/\pm57.5]$	1450						
					$[\pm57.5_3/90/\pm57.5/90_2]$	1532						
					$[\pm57.5_2/90/\pm57.5_2/90_2]$	1536						
					$[90/\pm57.5_2/90/\pm57.5_2/90]$	1565						
					$[90/\pm57.5/90/\pm57.5_3/90]$	1567						
					$[90/\pm57.5_3/90/\pm57.5/90]$	1632						
					$[90_2/\pm57.5_4/90]$	1664						
					$[90/\pm57.5_4/90_2]$	1775						
					$[\pm57.5/90/\pm57.5_3/90_2]$	1617						
scenario C[a] runtime = 20 min	0	7	–	–	$[90/\pm57.5_4/90_2]$	1503	2280	303	76	77%	–	6.1
					$[90_2/\pm57.5_4/90]$	1412						
					$[\pm57.5_4/90_3]$	1370						
					$[90/\pm57.5/90/\pm57.5/90]$	1386						
					$[\pm57.5/90/\pm57.5/90_3/57.5]$	1340						
					$[90/\pm57.5/90/\pm57.5_3/90]$	1331						
					$[57.5_3/90/\pm57.5/90_2]$	1309						
					$[\pm57.5_2/90/\pm57.5_2/90_2]$	1311						
					$[\pm57.5/90/\pm57.5_3/90_2]$	1375						
scenario D[a] runtime = 145 min	0	–	–	–	$[\pm62.5_5/90]$	1272	2208	265	74	75%	–	6.2
					$[90/\pm57.5_4/90_2]$	1503	2280	303	76	77%	–	6.1

(*Continued*)

scenario	constant				outputs							
	m_s (kg)	$p+q$	θ	W_f	lay-up config.	SN (Pa)	*HTS* (N/mm)	*LTS* (N/mm)	P_f (bar)	W_f	m_s (kg)	t (mm)
scenario D[b] runtime = 500 min	0	–	–	–	$[90_3/\pm67.5_6/90_3/\pm67.5]$	3134	4130	210	103	73%	–	9.5
					$[90_3/\pm62.5_6/90_4]$	3134	4029	313	101	74%	–	9.5
					$[90_3/\pm70_7/90_3]$	3150	4573	204	114	75%	–	9.5
					$[90_3/\pm55_6/90_4]$	3198	3861	506	96	76%	–	9.6
					$[90_2/\pm70_8/90_3]$	3172	5018	245	125	77%	–	9.5
scenario E[c] runtime = 115 min	75	–	–	–	$[\pm55_2/C/\pm55_3/90]$	5008	2023	431	77	77%	–	9.6
					$[\pm55_3/C/\pm55_2/90]$	5046						
scenario F[c] runtime = 840 min	–	–	–	–	$[\pm60_2/C/\pm60_2/90_2]$	5070	2099	262	70	77%	85	9.2
					$[\pm60_3/C/\pm60/90_2]$	5086						
					$[90/\pm60/C/\pm60_3/90]$	5095						
					$[90/\pm60_2/C/\pm60_2/90_1]$	5171						

Notes: a) for {600-16-1000} GFRP pipes; b) for {800-6-2500} GFRP pipes; c) for {600-16-4000} GFRP mortar pipes.

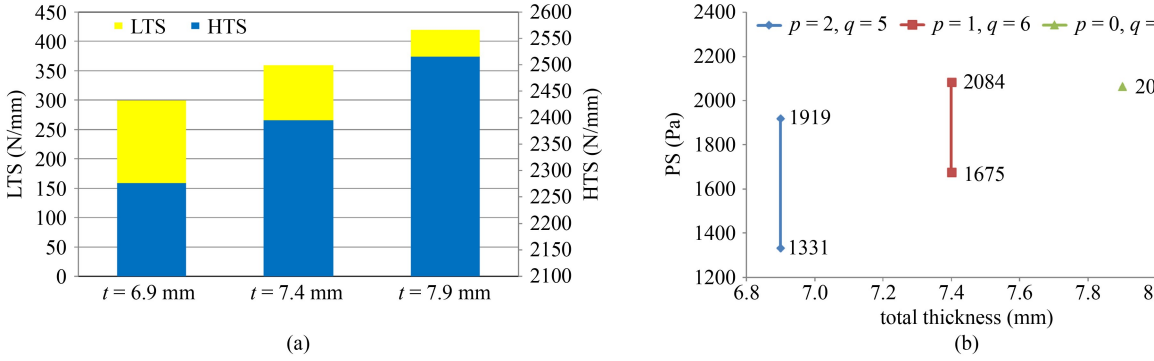

Fig. 4 Outputs of optimization for the scenario "A". (a) LTS and HTS; (b) pipe stiffness.

outputs among the 1152 alternatives of design patterns satisfy the design and manufacturing constraint requirements.

The green ovals in Fig. 5 imply the optimal design for scenario "B". Recalling from scenario "A", the minimum thickness is obtained as 6.9 mm, while the minimum thickness in scenario "B" is 6.5 mm. Unlike scenario "A", the combination of four cross and three hoop layers is resulted in the minimum thickness in scenario "B". The optimal design of the B-scenario is associated with a winding angle of 57.5°. In B-scenario, the best winding angle in the range of 50° to 70° is associated with 57.5° based on all design constraints for the fiber weight fraction of 73%. It is very well known that by increasing the winding angle, the thickness of cross layers decreases according to the Eqs. (5) and (6).

As shown in Fig. 5, for the minimum thickness of 6.5 mm, 16 different classes of pipe stiffness are obtained because of various admissible sequences of three hoops and four cross layers. The optimal design of scenario "B" consists of three hoops and four cross plies, while the optimal design of scenario "A" comprises two hoop and five cross layers. This stems from utilizing the optimal winding angle of 57.5° in scenario "B" compared to the

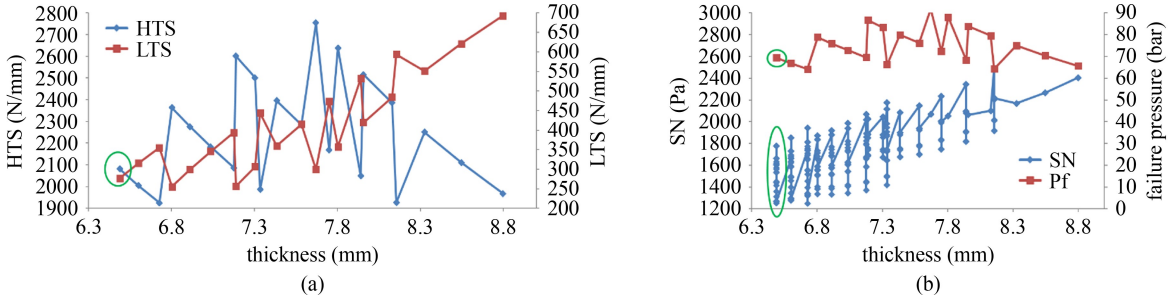

Fig. 5 Outputs of optimization for the scenario "B". (a) LTS and HTS; (b) pipe stiffness.

winding angle of 60° in scenario "A". The pipe stiffness for the optimal designs of the B-scenario varies from 1251 to 1775 Pa. Considering the maximum stiffness as the supplementary objective than the main objective of minimizing thickness, the best lay-up configuration would be $[90/\pm57.5_4/90_2]$.

6.2 Scenarios "C" and "D"

For the case of C-scenario, just the total number of layers is kept fixed and other design variables are varied according to Table 5. The influence of fiber weight fraction on the optimum winding angle is elaborated through this scenario for a GFRP pipe with 7 layers. The requirements of defined design constraints are met by 575 alternatives out of 5760 possible permutations. The thickness of the optimal designs as the outputs of C-scenario optimization is 6.1 mm. Different lay-up sequences are permissible for this minimum thickness, and thus nine different values for stiffness are identified. In all of these optimal designs circled in Fig. 6, both *HTS* and *LTS* have the same values as highlighted in green, while stiffness values are different. In Fig. 6, a part of outputs is shown avoiding messy illustration. The same as the outputs of the B-scenario, the combinations of four cross layers with a winding angle of 57.5° and three hoop layers lead to the optimal designs of the C-scenario. The pipe stiffness for the optimal designs of the C-scenario varies from 1309 to 1503 Pa. The latter is associated with the lay-up pattern of $[90/\pm57.5_4/90_2]$, like the output of the scenario "B".

In D-scenario, all restrictions are lifted, and the optimal design among all possible design patterns is intended to be found. Considering all reflected constraints in Table 5, 2230 design patterns are acceptable out of generated 22960 cases. In this scenario, the optimization procedure starts from the total layers of 2 and continues up to 8 layers. The optimal design for the GFRP pipe with {600-10-1000} specification through scenario "D" converges to the same optimal design reported by Scenario "C". Thus, the optimal design for this specific pipe {600-16-1000} is a 7-layer GFRP pipe (three hoop and four cross layers with winding angle of 57.5°) with fiber weight fraction of 77%. Some design patterns are acceptable for 6-layer GFRP pipes, but the thickness is higher than that of 7-layer pipes. The minimum thickness is associated with lay-up $[\pm62.5_5/90]$ and fiber weight fraction of 75%. Considering the main objective of the current optimization scenarios, i.e., minimizing the thickness, that 7-layer pipe is the optimal design. But, the 6-layer design configuration is also appealing because of less required cycle time for the production process of a 6-layer pipe than a 7-layer pipe.

The thickness variation trend in terms of fiber weight fraction and winding angle are shown in Fig. 7 as the outputs of optimization scenarios "C" and "D" for both optimum groups associated with 6- and 7-layer GFRP pipes with {600-16-1000} specification. It is worth mentioning that the presented data in Fig. 7 are associated with the minimum thickness avoiding messy figure, since different lay-up sequences are permissible for each combination of winding angle and fiber weight fraction. As can be seen in Fig. 7, for the fiber weight fraction of 73%–75%, the minimum thickness is associated with the winding angle of 62.5° for a 6-layer GFRP pipe, but for the fiber weight fraction of 76% and 77%, the optimal winding angle is adjusted to 57.5° and 55°, respectively. In contrast, for the 7-layer pipes, the minimum thickness occurs at the winding angle of 57.5° for all investigated fiber weight fractions, and similar trends are observed for them. This verifies the effect of winding angle and fiber weight fraction on the results.

Since the outputs of the optimization scenarios "C" and

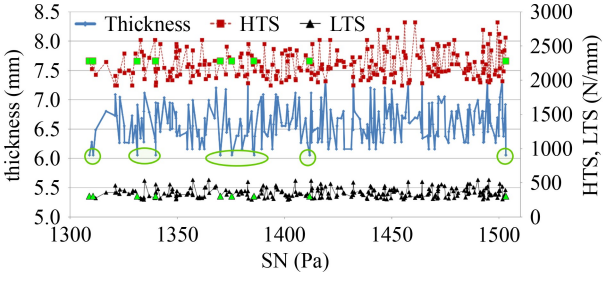

Fig. 6 Outputs of optimization for the scenario "C".

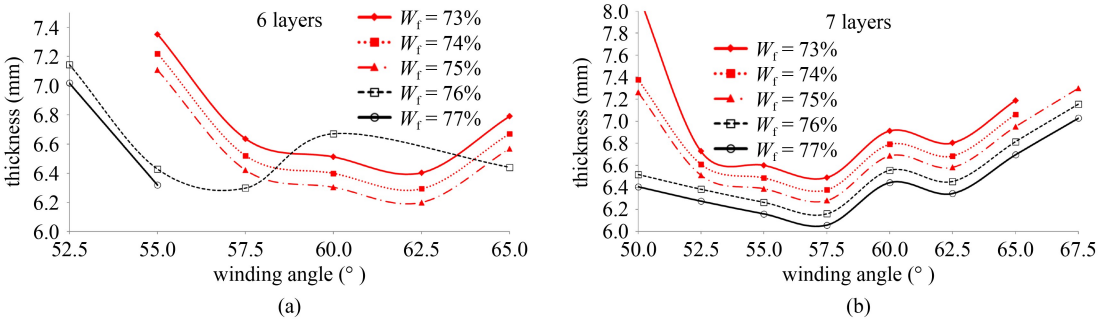

Fig. 7 Comparing variations of thickness versus winding angle for different fiber weight fraction as the output of optimization for {600-16-1000} GFRP pipes with (a) 6 and (b) 7 layers.

"D" coincide, the D-scenario is implemented on another GFRP pipe with {800-6-2500} specification to show the proficiency of the developed method without any KOE. It is interesting to observe that for this specific pipe, the obtained minimum thickness is the same for all fiber weight fractions, and five categories of the optimal design are found accordingly. Among the optimal designs of each category, those with maximum SN are inserted in Table 6. The optimal designs for the GFRP pipe with {800-6-2500} contain 13 layers, and the different optimal winding angle is obtained in cross plies for each fiber weight fraction.

6.3 Scenarios "E" and "F"

After implementing scenarios "A" to "D" on a GFRP pipe, the optimization is switched to the case of a GFRP mortar pipe. For this purpose, a GFRP mortar pipe with {600-10-4000} specification is chosen. This specific pipe requires a core layer to fulfil stiffness requirement. Because 6 or 7 GFRP layers can fulfill the *HTS*, *LTS*, and failure pressure constraints as discussed through the D-scenario. But, the thickness of the pipe is required to be increased to enhance stiffness. The industrial producers incorporate a core layer in-between the GFRP layers to increase the thickness of the pipe as an economical solution. In other words, increasing the thickness of GFRP pipes by utilizing extra redundant GFRP layers would lead to considerably high cost, and thus, required thickness is compensated by incorporating a core layer. In other words, the outputs of optimization for the D-scenario fulfills all design constraints for the {600-10-4000} GFRP mortar pipe except stiffness, and hence adding a core layer can satisfy this requirement as well.

In the E-scenario of optimization, 75 kg of sand is used to generate possible design patterns. In the F-scenario, the mass of sand is also considered a design variable. Since the amount of sand is considered as a constant value in the scenario "F", the thickness of the core layer is the same in all outputs of this scenario. The details of obtained results for all optimization mentioned above scenarios are presented in Table 6. The optimal designs in the E-scenario and F-scenario are totally different from optimal design in the D-scenario, despite the fact that the total numbers of the GFRP layers and fiber weight fraction are the same. Although the amount of incorporated sand has increased from 75 kg to 85 kg in the optimum design of the scenario "F", the thickness was reduced from 9.6 to 9.2 mm. This reduction is rooted in the optimal winding angle of 60° for this pipe.

It is very well known that accurate adjustment of fiber weight fraction is a formidable task in the reciprocal filament winding process of GFRP pipes from a practical point of view. The fiber weight fraction depends on various parameters like the applied tension to the fiber during the winding process, the wet ability of the fiber, TEX of the fiber, ambient temperature, the viscosity of resin and etc. On the other hand, a higher fiber weight fraction would always be led to the thinner GFRP pipes as a trivial output of Eqs. (1) and (5). Consequently, in those scenarios where fiber weight fraction is considered as a design variable (i.e., scenarios "C", "D", "E", and "F"), the optimal designs are associated with the maximum possible fiber weight fraction. It is emphasized that the code generates all possible cases for the whole range of defined fiber weight fractions, but just the optimum values are presented in Table 6.

7 Conclusions

Intending to attain the minimum achievable price, this research aims to develop an integrated design and optimization process to obtain the optimal customized structural design for GFRP pipes and GFRP mortar pipes. The application of investigated GFRP pipes is considered for conveying water and wastewater. The design constraints regulated by normative standards from short-term and long-term service viewpoints are identified. Then, proper computational tools are developed to predict the GFRP pipes' structural properties based on the lay-up configurations. The developed computational tools are validated through extensive experimental study, assuring the optimization foundation's proper performance. The developed computational procedures are quick and trustworthy enough since the optimization's runtime isinfluenced by these fundamental calculations. Then, the optimization framework is constructed by defining the minimum price as the primary objective and design requirements, and filament winding limitations as constraints. Design variables consist of the number of layers, lay-up sequence, fiber weight fraction, and winding angle for GFRP pipes, while for GFRP mortar pipe the amount of incorporated sand in the core layer is added to the list of variables as mentioned above, too. A computer code is written integrating design and optimization procedures. The optimization process is implemented through different scenarios to verify its proper performance. Firstly, pre-defined values are assumed for some design variables relying on the available KOE, and then involved design variables are added step-by-step to the optimization process untill no KOE is utilized.

The computer code needs pipe diameter, pressure class, and stiffness class as input data by the user and then optimal design(s) are presented based on the mechanical properties of fiber and resin. It can be applied for any new design even without background information on the structural pipe design in the form of KOE; however, the required runtime of analysis increases significantly. This

becomes even more pronounced when the number of layers increases in large diameter GFRP pipes and GFRP mortar pipes. Therefore, it is necessary to employ a meta-heuristic optimization technique without using KOE.

Acknowledgements The authors acknowledge the financial support provided by the Iranian National Science Foundation (INSF) under contract 4003139.

References

1. Nikbakt S, Kamarian S, Shakeri M. A review on optimization of composite structures Part I: Laminated composites. Composite Structures, 2018, 195: 158−185
2. Pan G, Lu J, Shen K, Ke J. Optimization of composite cylindrical shell subjected to hydrostatic pressure. In: International Conference on Intelligent Robotics and Applications. Cham: Springer, 2015, 81−90
3. Smerdov A A. A computational study in optimum formulations of optimization problems on laminated cylindrical shells for buckling I. Shells under axial compression. Composites Science and Technology, 2000, 60(11): 2057−2066
4. Diaconu C G, Sato M, Sekine H. Buckling characteristics and layup optimization of long laminated composite cylindrical shells subjected to combined loads using lamination parameters. Composite Structures, 2002, 58(4): 423−433
5. Foldager J P, Hansen J S, Olhoff N. Optimization of the buckling load for composite structures taking thermal effects into account. Structural and Multidisciplinary Optimization, 2001, 21(1): 14−31
6. Irisarri F X, Abdalla M M, Gürdal Z. Improved Shepard's method for the optimization of composite structures. AIAA Journal, 2011, 49(12): 2726−2736
7. Abouhamze M, Shakeri M. Multi-objective stacking sequence optimization of laminated cylindrical panels using a genetic algorithm and neural networks. Composite Structures, 2007, 81(2): 253−263
8. Kriegesmann B, Rolfes R, Jansen E L, Elishakoff I, Hühne C, Kling A. Design optimization of composite cylindrical shells under uncertainty. Computers, Materials & Continua, 2012, 32(3): 177−200
9. Rouhi M, Ghayoor H, Hoa S V, Hojjati M. Computational efficiency and accuracy of multi-step design optimization method for variable stiffness composite structures. Thin-walled Structures, 2017, 113: 136−143
10. Topal U. Multiobjective optimization of laminated composite cylindrical shells for maximum frequency and buckling load. Materials & Design, 2009, 30(7): 2584−2594
11. Wang Z, Almeida J H S Jr, St-Pierre L, Wang Z, Castro S G P. Reliability-based buckling optimization with an accelerated Kriging metamodel for filament-wound variable angle tow composite cylinders. Composite Structures, 2020, 254: 112821
12. M. Salim, M. Bodaghi, S. Kamarian, M. Shakeri. Free vibration analysis and design optimization of SMA/Graphite/Epoxy composite shells in thermal environments. Latin American Journal of Solids and Structures, 2018, 15(1): 1−16
13. Adali S, Walker M, Verijenko V E. Multiobjective optimization of laminated plates for maximum prebuckling, buckling and postbucklikng strength using continuous and discrerte ply angles. Composite Structures, 1996, 35(1): 117−130
14. Ameri E, Aghdam M M, Shakeri M. Global optimization of laminated cylindrical panels based on fundamental natural frequencies. Composite Structures, 2012, 94(9): 2697−2705
15. Ohta Y. Genetic algorithms for optimization of laminated composite cylindrical shells. In: 8th Symposium on Multidisciplinary Analysis and Optimization. Long Beach, CA: AIAA, 4939
16. Ohta Y. Optimal stacking sequence for nonlinear vibration of laminated composite circular cylindrical shells. In: 51st AIAA/ASME/ASCE/AHS/ASC Structures, Structural Dynamics, and Materials Conference 18th AIAA/ASME/AHS Adaptive Structures Conference. Orlando, FL: AIAA, 2010, 2882
17. Yas M H, Shakeri M, Khaksar N. Stacking sequence optimization of a composite cylindrical shell for vibrations by hybrid continuous optimization. Proceedings of the Institution of Mechanical Engineers. Part C, Journal of Mechanical Engineering Science, 2008, 222(12): 2385−2394
18. Luersen M A, Steeves C A, Nair P B. Curved fiber paths optimization of a composite cylindrical shell via Kriging-based approach. Journal of Composite Materials, 2015, 49(29): 3583−3597
19. Shakeri M, Yas M H, Gol M G. Optimal stacking sequence of laminated cylindrical shells using genetic algorithm. Mechanics of Advanced Materials and Structures, 2005, 12(4): 305−312
20. Correia I P, Martins P G, Soares C M, Soares C M, Herskovits J. Modelling and optimization of laminated adaptive shells of revolution. Composite Structures, 2006, 75(1−4): 49−59
21. Minsch N, Herrmann F H, Gereke T, Nocke A, Cherif C. Analysis of filament winding processes and potential equipment technologies. Procedia CIRP, 2017, 66: 125−130
22. Colombo C, Vergani L. Optimization of filament winding parameters for the design of a composite pipe. Composites. Part B, Engineering, 2018, 148: 207−216
23. Jin N J, Hwang H G, Yeon J H. Structural analysis and optimum design of GRP pipes based on properties of materials. Construction & Building Materials, 2013, 38: 316−326
24. Almeida J H S Jr, Ribeiro M L, Tita V, Amico S C. Stacking sequence optimization in composite tubes under internal pressure based on genetic algorithm accounting for progressive damage. Composite Structures, 2017, 178: 20−26
25. Liu C, Shi Y. Design optimization for filament wound cylindrical composite internal pressure vessels considering process-induced residual stresses. Composite Structures, 2020, 235: 111755
26. Zhang Z, Hou S, Liu Q, Han X. Winding orientation optimization design of composite tubes based on quasistatic and dynamic experiments. Thin-walled Structures, 2018, 127: 425−433
27. Alcántar V, Ledesma S, Aceves S M, Ledesma E, Saldana A. Optimization of type III pressure vessels using genetic algorithm and simulated annealing. International Journal of Hydrogen Energy, 2017, 42(31): 20125−20132
28. ANSI/AWWA C950-01. Standard for Fiberglass Pressure Pipe. Denver: American Water Works Association, 2001

29. Gibson R F. Principles of Composite Material Mechanics. 2nd ed. Boca Raton, FL: CRC Press, 2007
30. Roylance D K. Netting Analysis for Filament-wound Pressure Vessels. Watertown, MA: Army Materials and Mechanics Research Center, 1976
31. ASTM D2105-01. Standard Test Method for Longitudinal Tensile Properties of Fiberglass (glass Fiber Reinforced Thermosetting Resin) Pipe and Tube. West Conshohocken, PA: ASTM, 2001
32. ASTM D2290-00. Standard Test Method for Apparent Hoop Tensile Strength of Plastic or Reinforced Plastic Pipe by Split Disc Method. West Conshohocken, PA: ASTM, 2000
33. ASTM D1599-99. Standard Test Method for Resistance to Short-time Hydraulic Pressure of Plastic Pipes, Tubing, and Fittings. West Conshohocken, PA: ASTM, 1999
34. ASTM D2412-02. Standard Test Method for Determination of External Loading Characteristics of Plastic Pipe by Parallel-plate Loading. West Conshohocken, PA: ASTM, 2002
35. ASTM D3171-15. Standard Test Method for Constituent Content of Composite Materials. West Conshohocken, PA: ASTM, 2015
36. ASTM D2992-06. Standard Practice for Obtaining Hydrostatic or Pressure Design Basis for Fiberglass Pipe and Fitting. West Conshohocken, PA: ASTM, 2006
37. ISO 10468. Glass-reinforced Thermosetting Plastics (GRP) Pipes—Determination of the Ring Creep Properties Under Wet or Dry Condition. Genewa: ISO, 2018
38. Rafiee R, Ghorbanhosseini A. Developing a micro-macro mechanical approach for evaluating long-term creep in composite cylinders. Thin-walled Structures, 2020, 151: 106714
39. Rafiee R, Ghorbanhosseini A. Experimental and theoretical investigations of creep on a composite pipe under compressive transverse loading. Fibers and Polymers, 2021, 22(1):222–230
40. Rafiee R, Ghorbanhosseini A. Analyzing the long-term creep behavior of composite pipes: Developing an alternative scenario of short-term multi-stage loading test. Composite Structures, 2020, 254: 112868
41. Rafiee R, Mazhari B. Simulation of long-term hydrostatic tests on glass fiber reinforced plastic pipes. Composite Structures, 2016, 136: 56−63
42. Rafiee R, Mazhari B. Evaluating long-term performance of glass fiber reinforced plastic pipes subjected to internal pressure. Construction & Building Materials, 2016, 122: 694−701
43. Shaaban A M, Anitescu C, Atroshchenko E, Rabczuk T. An isogeometric Burton-Miller method for the transmission loss optimization with application to mufflers with internal extended tubes. Applied Acoustics, 2022, 185: 108410
44. Shaaban A M, Anitescu C, Atroshchenko E, Rabczuk T. 3D isogeometric boundary element analysis and structural shape optimization for Helmholtz acoustic scattering problems. Computer Methods in Applied Mechanics and Engineering, 2021, 384: 113950
45. Shaaban A M, Anitescu C, Atroshchenko E, Rabczuk T. Isogeometric boundary element analysis and shape optimization by PSO for 3D axi-symmetric high frequency Helmholtz acoustic problems. Journal of Sound and Vibration, 2020, 486: 115598
46. Shaaban A M, Anitescu C, Atroshchenko E, Rabczuk T. Shape optimization by conventional and extended isogeometric boundary element method with PSO for two-dimensional Helmholtz acoustic problems. Engineering Analysis with Boundary Elements, 2020, 113: 156−169
47. Ghasemi H, Park H S, Rabczuk T. A multi-material level set-based topology optimization of flexoelectric composites. Computer Methods in Applied Mechanics and Engineering, 2018, 332: 47−62
48. Ghasemi H, Park H S, Rabczuk T. A level-set based IGA formulation for topology optimization of flexoelectric materials. Computer Methods in Applied Mechanics and Engineering, 2017, 313: 239−258